Original Study **Open Access**

Šarūnas Skuodis, Neringa Dirgėlienė*, Jurgis Medzvieckas

Using Triaxial Tests to Determine the Shearing Strength of Geogrid-Reinforced Sand

https://doi.org/10.2478/sgem-2020-0005
received March 16, 2020; accepted July 16, 2020.

Abstract: Geogrids are widely used in civil engineering projects to reinforce road and railway structures. This paper presents research on the shearing strength of soil samples that have been reinforced with geogrids. The relationship between soil and geogrids is explored and evaluated by modeling the mechanical behavior of heterogeneous materials. For the purposes of this research, data obtained from tests of unreinforced sand samples with triaxial cells were compared with the data obtained from tests of reinforced sand samples. It was found that the shearing strength for reinforced samples was higher (from 9% to 49%) compared to unreinforced samples. Some damage to the geogrid was detected during the experiment, and for this reason, the same tests were numerically simulated for both unreinforced samples and samples reinforced with geogrids. Numerical simulations revealed the main reasons for damage to the geogrids during triaxial testing.

Keywords: geogrid; sand; shearing strength; angle of internal friction; cohesion.

List of notations

σ	normal stresses
τ	tangential stresses
φ'	effective angle of internal friction
c'	effective cohesion
σ_3	cell pressure
$\sigma_1-\sigma_3$	max stress deviator
ε	vertical strain
E	Young's (elastic) modulus

***Corresponding author: Neringa Dirgėlienė,** Department of Reinforced Concrete Structures and Geotechnics, Vilnius Gediminas Technical University, Saulėtekio al. 11, LT-10223 Vilnius, Lithuania, E-mail: neringa.dirgeliene@vgtu.lt
Šarūnas Skuodis, Jurgis Medzvieckas, Department of Reinforced Concrete Structures and Geotechnics, Vilnius Gediminas Technical University, Saulėtekio al. 11, LT-10223 Vilnius, Lithuania

1 Introduction

Geogrid is a geosynthetic material used as reinforcement in construction works, which increases the bearing capacity and equalizes displacements in sand conditions.[1–4] Geogrid typically includes a mixture of polypropylene (PP), high-density polyethylene (HDPE), and polyester (PET). Geogrid can be either flexible or rigid in nature; the manufacturing process, manufacturing technology, and the behavior of grids will vary depending on the type of synthetic materials used. Thus, it is important to understand the technical specifications for a particular geogrid.

One of the main properties of geogrids is its nominal tensile strength in both a machine direction and a cross-machine direction. The declared geogrid tensile strength depends on the degree of strain. This is important to know when evaluating the use of geogrids as soil reinforcement. Usually, the strength values of design geogrids are calculated according to the strain: 1%, 2%, 5%, and 10%. Strains in excess of 10% require the use of typical tensile strength and strain curve.[5] The design value of tensile strength is determined during the geogrid tests when loads and strains are being measured, although it is important to note that tests are performed on the geogrid without any interaction with the surrounding soil.

In general, all of the necessary geogrid properties are evaluated with partial safety factors[6–8] whose application ensures safety of the entire geotechnical construction, which is reinforced with geogrid during storage, installation, loading, durability, etc.[8]

Research conducted in recent decades has shown that different types of geosynthetic reinforcements are widely used to improve the shear strength of soil materials. Such research has identified the main factors affecting mechanical behavior, including the number of geotextile layers, their arrangement in specimens, confining pressure, particle size distribution, geotextile type, and the relative density of samples. Diverse experimental approaches have investigated the productive effects of geotextile reinforcement in geotechnical projects. Some researchers employed full-scale, reduced scale

models of geotextile-reinforced soil or an experimental approach, such as compression triaxial and direct shear equipment, to evaluate the effects of reinforced horizontal geosynthetic layers in soil. Nair and Latha[9] carried out triaxial experiments with granular subbase samples reinforced with multiple layers of geogrid and geotextile reinforcements. They concluded that reinforced systems carried more stresses than unreinforced systems at the same strain level. The benefit of geocell reinforcement was evident only at high strains, whereas planar reinforcement was effective at much lower strain levels. Stiffness reduction was found to be low for geocell-reinforced samples compared with the samples reinforced with planar layers of geogrid. Sakleshpur et al.[10] indicated that the improvement in shear strength of an unreinforced soil aggregate sample due to the placement of biaxial geogrid with an aperture of 33 × 33 mm and a tensile strength of 4 kN/m at 2% strain at the interface is greater for relatively softer subgrades compacted at water content above the optimal than for subgrades compacted at the optimal water content. Large-scale direct shear tests were conducted to study the interaction between sand and 3-D geogrid under direct shear mode. Medium and fine fractions of clean, dried river sand were used in the study. Compared to planar geogrid, a 16% and 22% improvement in interface shear strength was provided by medium sand reinforced with 3-D geogrids of triangular and rectangular pattern, respectively. The interface shear strength coefficient of 3-D geogrid-reinforced fine sand was lower compared to 3-D geogrid-reinforced medium sand.[11] Other researchers have performed the triaxial tests on reconstituted specimens of dry, natural sand prepared at a loose relative density (Dr = 30%) with and without geotextile layers and consolidated to three levels of confining pressures, 50, 100, and 200 kPa, where differing numbers and arrangements of reinforcement layers were placed at different heights of the specimens (zero, one, and two layers). The geotextile inclusion improves the mechanical behavior of sand; thus, a significant increase in the shear strength and cohesion value is obtained by adding layers of reinforcement. Also, the results indicate that the value of the strength ratio is bigger for samples which are subjected to a low value of confining pressure. The results obtained reveal that a high value of confining pressure can restrict the sand dilatancy when shearing.[4] A series of consolidated undrained triaxial compression tests for investigating the shear behavior of geotextile-reinforced clay were conducted. The experimental results revealed that during consolidation, non-woven geotextile as a permeable material reduced the time of consolidation; however, it induced a higher volume change. During undrained loading, the shear strength and excess pore water pressure of the reinforced clay increased with the number of geotextile layers due to the restraint of the lateral deformation resulting from the mobilized tensile force of reinforcement layers. This study demonstrated that the reinforcement is more effective in enhancing additional confining pressure than increasing excess pore water pressure. [12]

Drained triaxial tests on encased and non-encased samples of gravel were performed to study the influence of encasement on the behavior of stone columns. This improvement is more significant for low confining pressure.[13] Different layers of reinforcements including one, two, and three geotextile layers were placed in the reinforced calcareous soil samples and sheared in drained conditions. The results show that confining pressure has a significant effect on the efficiency of reinforcements. It is evident from this study that increasing the reinforcement layers decreases the particle breakage of the calcareous soils.[14] To make a precise comparison between the behavior of reinforced siliceous and carbonate sand, the authors performed triaxial tests on both types of sands. Results indicated that geotextile inclusion increases the peak strength and strain at failure and significantly reduces the post-peak strength loss of carbonate specimens. The strength enhancement of reinforced carbonate sand is greater than the corresponding siliceous sample at high axial strains.[15]

Thus, the purpose of this article is to determine the shearing strength of quartz sand reinforced with flexible and rigid geogrids by using the triaxial compression test. Numerical modeling provided a better understanding of the distribution of stress in the soil specimen reinforced with geogrid, especially in the plane with geogrid. Numerical analysis also showed the influence of geogrids on stress–strain distribution in soil samples.

2 Experimental setup

2.1 Soil properties

The mineralogical composition of sand used for investigation was determined by Amšiejus et al., wherein sand was found to contain ~85% of quartz and ~6% of feldspar, with the remaining part contributed by carbonate, mica, and some other minerals.[16] The determined density of particles was ρ_s = 2.65 g/cm^3. The sphericity of investigated soil particles was quite high (S_{2D} = 0.836), and the form coefficient was $K_{f,2D}$ = 0.702.[17] According to

Table 1. The main properties of flexible and rigid geogrids (taken from the technical brochures of suppliers).

Properties	Basetrac® Grid PP 40	Secugrid 40/40 Q1	Basetrac® Grid PET 40
Nominal tensile strength (machine direction), nominal tensile strength (cross-machine direction)	≥40 kN/m	≥40 kN/m	≥40 kN/m
Strain at nominal tensile strength	7%	7%	10%
Durability	Predicted to be durable for a minimum of 100 years in natural soils with 4 ≤ pH ≤ 9 and soil temperatures ≤25 C if covered within 30 days after installation	Predicted to be durable for a minimum of 100 years in natural soils with 4 ≤ pH ≤ 9 and soil temperatures ≤25 C if covered within 30 days after installation	Predicted to be durable for a minimum of 100 years in natural soils with 4 ≤ pH ≤ 9 and soil temperatures ≤25 C if covered within 30 days after installation

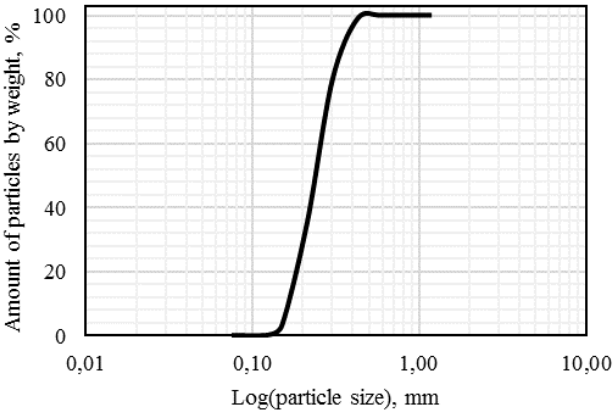

Figure 1. Granulometric curve of the investigated soil.

the granulometric curve (Fig. 1), the soil investigated was uniformly graded sand, the uniformity coefficient was C_U = 1.47, and the coefficient of curvature was C_C = 0.93. The soil granulometric composition revealed 1.34% fine sand, 96.38% medium sand, and 2.28% coarse sand particles, determined according to ISO 14688-1:2017.[18] Particles of this soil are mostly of the same shape because it is sampled from the Klaipėda seashore, where the surface particles have been polished by the action of waves. Also, this sand does not contain silt, clay, and gravel additives. For the purposes of scientific testing, Klaipėda sand from the Baltic Sea is called Lithuanian standard sand due to its granulometric composition and particle shape.[19] After the tests, it was found that there was no effect of crushing of soil particles.[20,21]

Triaxial tests for this soil with and without geogrid reinforcements were conducted. The results obtained were compared while evaluating the ratio of reinforced and unreinforced soil samples.[22] This research did not analyze the effects of particle size on the interfacial shear strength.[23,24]

2.2 Geogrid properties

This study analyzed the most commonly used geogrid types in Lithuania.[25] The flexible Basetrac® Grid PP 40 and Basetrac® Grid PET 40, and also rigid Secugrid 40/40 Q1 geogrids were used to compare the geogrids. The main properties of flexible and rigid geogrids are given in Table 1.

The purpose of this article is to evaluate the thread form of geogrids and the influence of mesh size on stress distribution in the sample and character of the failure plane. Basetrac Grid PP 40 is made of three round alongside threads with a mesh size of 30 × 30 mm. The sample cross section contained a single mesh. Basetrac Grid PET 40 is made of two round alongside threads, whose mesh size is 25 × 25 mm. The sample cross section contained four meshes. Secugrid 40/40 Q1 geogrid is made of one flat thread and the mesh size is 30 × 30 mm. The sample cross section contained one mesh.

Geogrids must be anchored in the surrounding soil mass; a small part placed in the middle of the triaxial sample is a rigid element compared with the soil. The actual mechanical properties of a geogrid's element are not relevant because only a small piece is placed in the sample. The strength and elongation stiffness of the geogrid's element are much higher than those of soil.

2.3 Triaxial test procedure

Triaxial tests were carried out using samples of 100 mm in diameter and 200 mm in height. Due to boundary conditions, it is suggested in the literature to test samples of height h and diameter d in the ratio h/d = 2.[26] The tests were chosen to run under isotropic, unsaturated, consolidated, and drained conditions.[27] The conditions of these tests simulate the natural exploitation environment

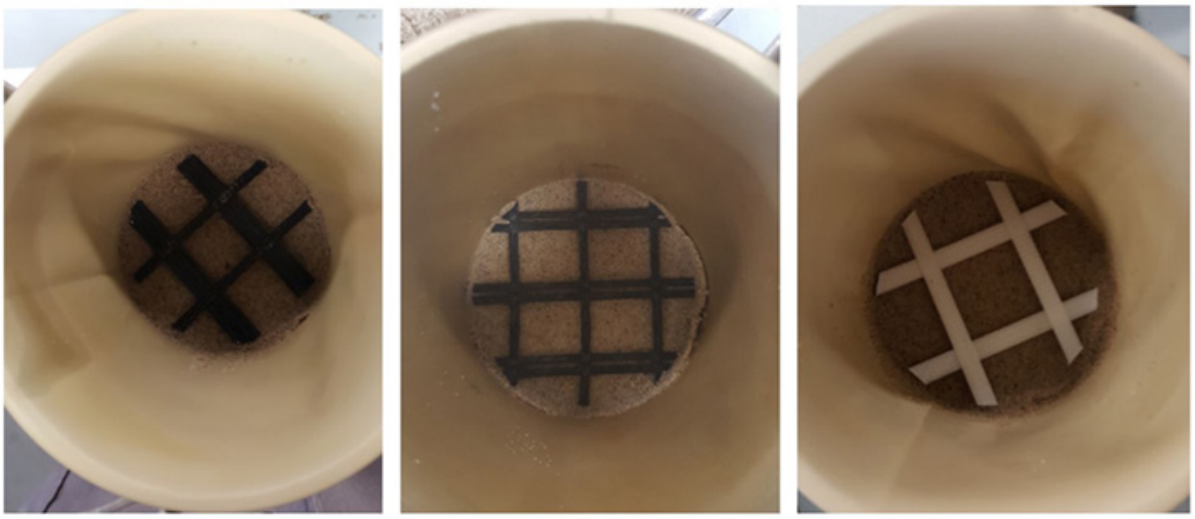

Figure 2: Sample reinforcement with geogrid: left – flexible Basetrac® Grid PP 40 geogrid; middle – flexible Basetrac® Grid PET 40 geogrid; right – rigid Secugrid 40/40 Q1 geogrid.

Table 2: Density of investigated samples.

Sample	Density, g/cm³
Unreinforced	1.72–1.73
Basetrac® Grid PP 40	1.67–1.69
Secugrid 40/40 Q1	1.69–1.70
Basetrac® Grid PET 40	1.69–1.72

of geotechnical constructions of roads and railways. All samples were prepared with an initial water content of w = 6.0% by compacting in 10 layers. This water content represents roadbed moisture. The geogrid was pressed gently into the sand. All samples were consolidated for 30 min, and according to the consolidation time, the vertical strain velocity 0.950%/min was calculated. Each of the tests was continued up to maximal deformation, which is equal to 15.0%. When choosing the cell pressure, there was no special simulation of any case study or existing project, so the experiments used the following cell pressures: σ_3 = 100, 200, and 300 kPa. All investigated soil samples were prepared with a density as uniform as possible (see Table 2). The void ratio of samples was approximately e = 0.65, and the saturation degree was Sr = 25%.

The density of initial samples did not differ to any significant degree because during triaxial testing for soil sample reinforcement, only one layer of geogrid was used (Fig. 2). The geogrid was positioned directly in the middle of the sample, exactly 100 mm from the top and bottom. Tests with more than one reinforcing geogrid layer were not carried out because according to Kamel and Chandra,[28] the most significant geogrid influence is obtained when one geogrid layer is used for triaxial sample reinforcement.

2.4 Interpretation of results

The peak shearing strength for unreinforced and reinforced soil samples was determined by the maximum ratio of tangential and normal stresses $\tau/\sigma' = \max$. For unreinforced soil samples, the Mohr–Coulomb criterion $\tau = \sigma' \tan\phi' + c'$ was applied. Line parameters such as the angle of internal friction $\tan\phi'$ and cohesion $c¢$ were determined by using the least squares method. The Mohr–Coulomb failure criterion was also applied to evaluate the peak shearing strength of samples reinforced with geogrids. Most of the reinforced soil samples exhibited apparent cohesion, so the Mohr–Coulomb equation was used to calculate the shear strength improvement of the geosynthetic reinforced soil composites. In this case, the influence of geogrid on shearing strength was evaluated as with apparent cohesion c' and the friction angle of geosynthetic reinforced soil with $\tan\varphi'$.[22]

3 Analysis of experimental results

Firstly, soil tests without any geogrid reinforcement were performed. The sample failure shape obtained was very common with the shapes presented in the literature.[29–31] Next, a series of tests was carried out with samples reinforced using flexible and rigid geogrids. In this case,

Figure 3: Sample failure shape (from left to right): unreinforced; reinforced with Basetrac® Grid PP 40 geogrid; reinforced with Basetrac® Grid PET 40 geogrid; reinforced with Secugrid 40/40 Q1 geogrid.

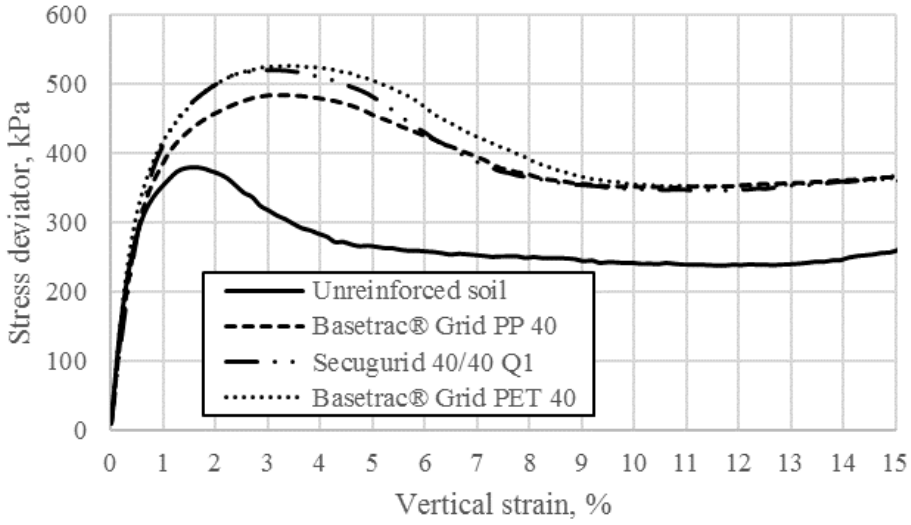

Figure 4: Dependence of stress deviator on the vertical strain of unreinforced and reinforced soil samples with geogrids when the cell pressure σ_3 = 100 kPa.

the sample failure shape was not the same where there was no reinforcement (see Fig. 3).

For samples with no geogrid reinforcement, the failure plane was obtained from the top of the sample to its bottom, with the failure shape corresponding to the theoretical dependence with the angle of internal friction. The shape was not valid for samples reinforced with geogrids; instead, soil samples reinforced with flexible and rigid geogrids produced up to 10 failure planes which started from the top of the sample and extended to the geogrid positioned in the middle of the sample. For this reason, the measured max stress deviator (σ_1–σ_3) values were higher for samples reinforced with geogrids. Dependence of stress deviator on the vertical strain of unreinforced and reinforced soil samples with geogrids is presented in Figs 4–6.

From the results presented in Figs 4–6, it is evident that when the cell pressure σ_3 = 100 and 200 kPa, the resistance and residual strength of samples reinforced with flexible or rigid geogrids are much more higher than unreinforced samples. The flexible geogrids Basetrac Grid PP 40 and Basetrac Grid PET 40 and rigid Secugrid 40/40 Q1 are equivalent in their reinforcing properties (Table 1) because the nominal tensile strength ≥40 kN/m is the same for all geogrids investigated. When the cell pressure is σ_3 = 300 kPa, resistance of the unreinforced sample at peak

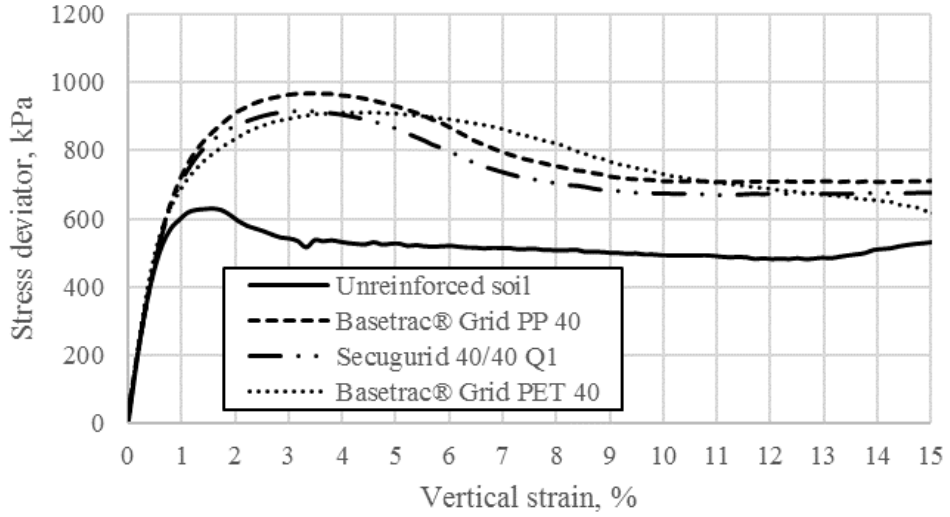

Figure 5: Dependence of stress deviator on the vertical strain of unreinforced and reinforced soil samples with geogrids when the cell pressure σ_3 = 200 kPa.

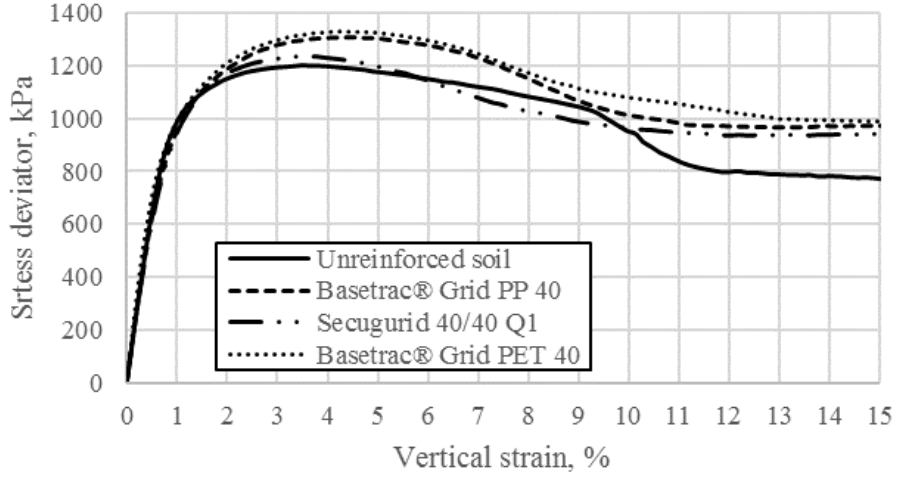

Figure 6: Dependence of stress deviator on the vertical strain of unreinforced and reinforced soil samples with geogrids when the cell pressure σ_3 = 300 kPa.

strength is almost similar to that of reinforced samples with geogrids. This phenomenon can be explained by the high cell pressure applied (σ_3 = 300 kPa) during the test. High cell pressure has an influence on stress distribution in the sample.[32] Nevertheless, residual strength of unreinforced samples is smaller than that of reinforced samples, when the cell pressure is σ_3 = 300 kPa. See Table 3 for a detailed comparison of peak shearing strength. Residual shearing strength results were already reported by Skuodis and Dirgėlienė.[33]

On comparing the peak shearing strengths presented in Table 3, it is evident that unreinforced soil samples reach peak shearing strength at twice smaller vertical strain when compared with reinforced soil samples with geogrids. This tendency is valid only for soil samples tested under the cell pressure σ_3 = 100 and 200 kPa. When the cell pressure is σ_3 = 300 kPa, the difference is not so obvious. It is noticeable that by increasing the confining pressure, the geogrid reinforcement effect on the sand sample decreases. Geotextile has low productivity at a high confining pressure, yet the shear strength is considerably increased at a low confining pressure. Geotextile layer decreases the dilative behavior of sand and has a confining effect on specimens. In high confining pressures, the geotextile has a low confining effect on specimens, which leads to a low increase in the shear strength.[15]

Table 3: Unreinforced and reinforced soil with geogrid shearing strength.

Peak strength						
Test conditions	**Cell pressure σ_3, kPa**	**Max stress deviator $\sigma_1-\sigma_3$, kPa**	**Vertical strain ε, %**	**Angle of internal friction ϕ', °**	**Cohesion c', kPa**	**Shearing strength ratio (reinforced/unreinforced)**
Unreinforced	104.54	380.67	1.5810	40.77	0.00	-
	202.98	627.85	1.5758			-
	305.39	1202.45	3.4799			-
Basetrac® Grid PP 40	106.68	484.87	3.3234	42.28	22.82	1.31
	204.78	966.78	3.4615			1.31
	305.30	1308.82	4.4283			1.12
Secugrid 40/40 Q1	106.20	521.38	3.0033	39.78	43.47	1.43
	205.65	916.87	3.3232			1.31
	305.13	1233.04	3.6346			1.09
Basetrac® Grid PET 40	107.01	526.76	3.3171	41.90	20.27	1.32
	206.10	908.43	5.0638			1.27
	306.44	1328.61	4.1152			1.11

The cohesion evaluated for soil samples reinforced with geogrids should be interpreted as apparent cohesion c_a.[22] Normally, for noncohesive soils reinforced with geogrids, some values of cohesion are established.[28]

Also investigated in this study was the wear of geogrids before and after tests. Irregularities were obtained for the flexible Basetrac Grid PP 40 and the rigid Secugrid 40/40 Q1 geogrids; however, some changes in geogrid condition were observed before and after triaxial tests for Basetrac Grid PET 40 geogrid (see Fig. 7).

Fig. 3 shows that Basetrac Grid PET 40 geogrid has four openings. This means that such connections are orientated close to the external surface of the sample. It is in this zone that the higher stress deviator values appear during tests, which leads to some damage to geogrid connections. The other two geogrids investigated (flexible Basetrac Grid PP 40 and rigid Secugrid 40/40 Q1) have only one opening, in which case the geogrid connections are located close to the middle of the sample where the stress deviator is lower than at the edge of the sample cross section. This explains why there was no damage to flexible Basetrac Grid PP 40 and rigid Secugrid 40/40 Q1 geogrid connections. The numerical simulation section (Section 4) presents a detailed explanation of damage to geogrid connections.

4 Analysis of numerical simulation results

Numerical modeling is used to evaluate the processes that take place in soil and the nature of these processes.[34] Numerical simulation of triaxial tests was achieved using the PLAXIS 3D program which evaluates stress distribution in the simulated sample, especially in the plane with the geogrid. A small portion of the geogrid is rigid and inserted with a small deformation in comparison with the soil. The calculated stiffness of such small geogrid fragments will be almost equal. Hence, for small geogrid fragments, the concept of flexibility does not apply. For this research, the essential factor is the amount of geogrid lines in the cross section of the sample. The sample size for numerical simulation chosen was 10 times the size of the real sample, which was possible when model dimensions were entered using the SI system unit, meter (m). When the sample size is chosen in meters, the stresses are given in kilopascals, which makes it easier to evaluate their size and nature of their distribution. The strong correlation with actual experimental tests results confirms the suitability of the choice. Standard soil tests were simulated and the results were compared with those from actual laboratory tests. The shape and dimensions of the numerical model corresponded to the laboratory sample. A plastic calculation was used to conduct an elastic–plastic deformation analysis according to

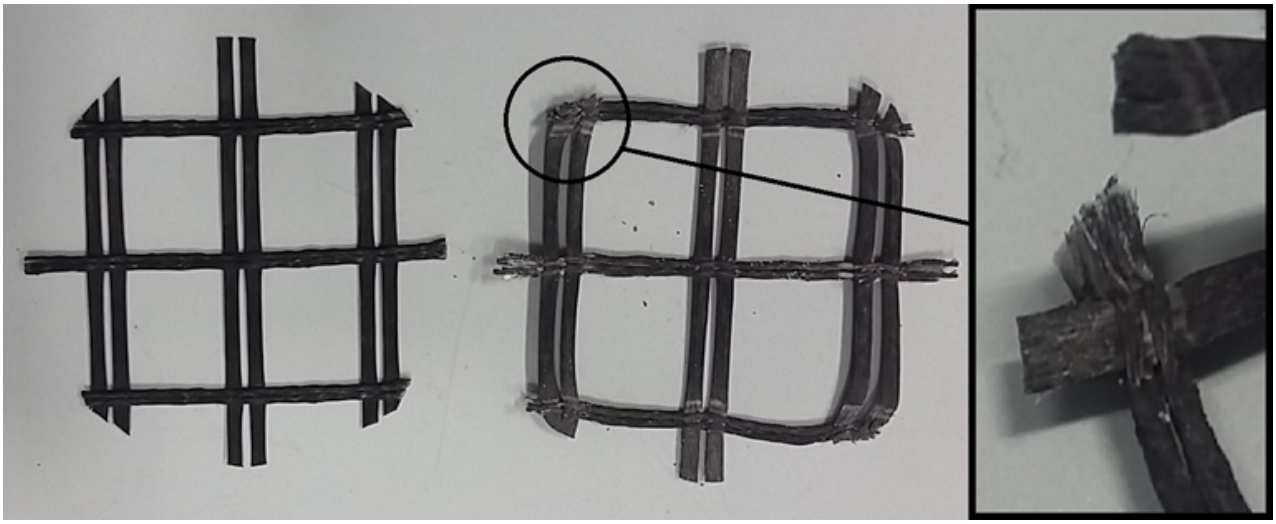

Figure 7: Basetrac® Grid PET 40 geogrid condition: left – geogrid without damages before test; right – geogrid damages after test.

small deformation theory. After defining the initial phase, the numerical test was modeled and compressed isotropically using confining pressure σ_3. Next, the axial pressure σ_1 was increased, while the radial pressure σ_3 was kept constant. The distributed loads on vertical and horizontal planes were used to model pressure σ_3 and σ_1. Different pressure σ_1 levels were activated in each calculation phase. Following the successful completion of a calculation phase, a new phase with increased pressure σ_1 was initiated. For an unsuccessful calculation, a failure situation was indicated. The last value of pressure σ_1 of the modeled numerical tests can be seen in Table 4.

Stress states at failure are described using the Mohr–Coulomb failure criterion. The elastic–plastic Mohr–Coulomb model involves effective strength parameters: angle of internal friction φ', cohesion c', dilatancy angle Ψ for soil plasticity, effective stiffness parameter Young's modulus E', and Poisson's ratio ν' for soil elasticity. In the finite element program PLAXIS, the exact form of the full Mohr–Coulomb model is implemented using a sharp transition from one yield surface to another.[35] For stress states within the yield surface, the behavior is elastic. For simulation, soil parameters such as the angle of internal friction φ' = 41̊, cohesion c' = 1 kPa, dilatancy angle Ψ = 9, Young's modulus E' = 40 MPa, and Poisson's ratio ν' = 0.3 were applied. The software developers recommend taking the value of the cohesion, but not zero, i.e. slightly higher than zero. The dilatancy of sand depends on both density and the angle of internal friction. For sand, the magnitude of the angle of dilatancy is about $\Psi = \varphi' - 30°$.[36] The calculations performed under drained conditions means that the influence of water was not evaluated.

Numerical simulations provided for two different types of geogrids: Basetrac Grid PP 40 and Basetrac Grid PET 40, which were simulated because they have different number of openings in the triaxial sample cross section. It is difficult to assess the exact difference between the flexible Basetrac Grid PET 40 geogrid and the rigid Secugrid 40/40 Q1 geogrid with the same grid openings, so rigid Secugrid 40/40 Q1 geogrid was not simulated. The shape of simulated geogrids, their dimensions, and cross-sectional area were in accordance with the data from experiments and based on the scale 1:10 (the same magnification as for the sample size).

The main problem in the numerical simulation appears when assigning a modulus of elasticity for the geogrid. The tensile modulus of the PP is about 1.2 GPa; in another source, it is given as 1.3–14.9 GPa.[37,38] The PLAXIS 3D program contains models for the linear and nonlinear behavior of structural elements. The authors of this paper chose the linear behavior for geogrid elements. Since the area of the geogrid fragment occupies a considerable cross-sectional area of the sample, the plate elements (in PLAXIS-named floor) are used to model geogrid elements. The area occupied by the geogrid fragments is presented in Figs 9, 12, and 13 (area marked in green). The width (b = 7.0 × 10 mm) of the geogrid lines corresponded to the numerical simulation ratio. The behavior of these elements is defined using elastic stiffness properties. The floor element is used to model horizontal (two-dimensional) structures in the ground with significant rigidity (bending stiffness). Before the creation of geogrid fragments, the corresponding contour needs to be created using geometry lines. The basic parameters include the thickness (for the numerical simulation, d = 1.0 × 10 mm),

Table 4: Simulated unreinforced and reinforced soil shearing strength with PLAXIS 3D.

Test conditions	Experimental results		Simulation	
	Cell pressure σ_3, kPa	Max stress deviator $\sigma_1-\sigma_3$, kPa	Cell pressure σ_3, kPa	Max stress deviator $\sigma_1-\sigma_3$, kPa
Unreinforced	104.54	380.67	100.0	365.0
	202.98	627.85	200.0	740.0
	305.39	1202.45	300.0	1110.0
Basetrac® Grid PP 40	106.68	484.87	100.0	470.0
	204.78	966.78	200.0	960.0
	305.30	1308.82	300.0	1410.0
Basetrac® Grid PET 40	107.01	526.76	100.0	510.0
	206.10	908.43	200.0	910.0
	306.44	1328.61	300.0	1460.0

unit weight of the floor material, Young's modulus, shear modulus, and Poisson's ratio (ν_{12} = 0.1). Distinct stiffness can be specified for a different floor direction by selecting the model parameters E_1 and E_2. Young's modulus was accepted to be equal in both directions ($E_1 = E_2 = 5.7 \times 10^7$ kPa). The shear modulus is related to the Young's modulus according to Hooke's law of isotropic elasticity. The element allows for plane deflection due to shearing, as well as bending and changes in length when axial forces are applied. The basic material parameters should be chosen in such a way that the resulting stiffness would be equivalent to the stiffness of the small geogrid element. Geometric dimensions should match the selected model ratio, in which event the resulting rigidities and shear stiffness of the geogrid element should be dependent on the chosen value of Young's modulus. The small element of the geogrid is a highly rigid insert with a small deformation in comparison with the soil. In this case, different calculations were conducted with various values, i.e. 5.7×10^5, 5.7×10^6, and 5.7×10^7 kPa. A perfect match with experimental test results was obtained when the simulated geogrid modulus of elasticity was 5.7×10^7 kPa. After finding all matches for numerical and experimental tests, an assumption was made that the stress state in the numerical model is equal to the stress state in the real sample. From numerical simulations, the stress deviator values ($\sigma_1-\sigma_3$) at the sample failure were found (Table 4).

Distribution of the stress deviator in the vertical and horizontal cross section at the failure stage of the samples is given in Figs 8 and 9. Here, porous stone influence at the top and bottom of the sample horizontal strain restriction on unreinforced soil is obtained and additional influence on the middle of the cross section of reinforced samples with geogrid is indicated.

Analysis of the distribution of stress deviators presented in Figs 8 and 9 shows that maximum stress deviator concentrates in the zones where there is no reinforcement. Smaller stress deviators are obtained where the sample comes into contact with porous stone and also in the zone of reinforcement with the geogrid. At the point of failure, the ultimate stress deviator zone is much larger in the unreinforced sample. The distribution of approximately uniform stresses is more flat in the reinforced specimen. The area of ultimate stress deviators is much smaller, but the stresses are much larger (Fig. 8), the distribution of which depends on the amount of reinforcement in the cross section. For the sample reinforced with Basetrac Grid PET 40 geogrid, distribution of the stress deviator is more uniform in the entire cross section.

Stress deviator increment appears in the geogrid connections, which damaged the Basetrac Grid PET 40 geogrid connections during experimental testing. Maximum axial tension forces appear in the middle of cross section (Fig. 10).

Maximum tension forces appear in the middle of the cross section when the Basetrac Grid PET 40 geogrid is simulated. For different cell pressures (σ_3 = 100 and 300 kPa), average tension forces which form in geogrids difference are minimal. In geogrid tape (which is in the center of the cross section), extreme tensile force is present; but this decreases when the geogrid tape is moved away from the center of the cross section. Maximum shear forces appear at the geogrid's connections (Fig. 11).

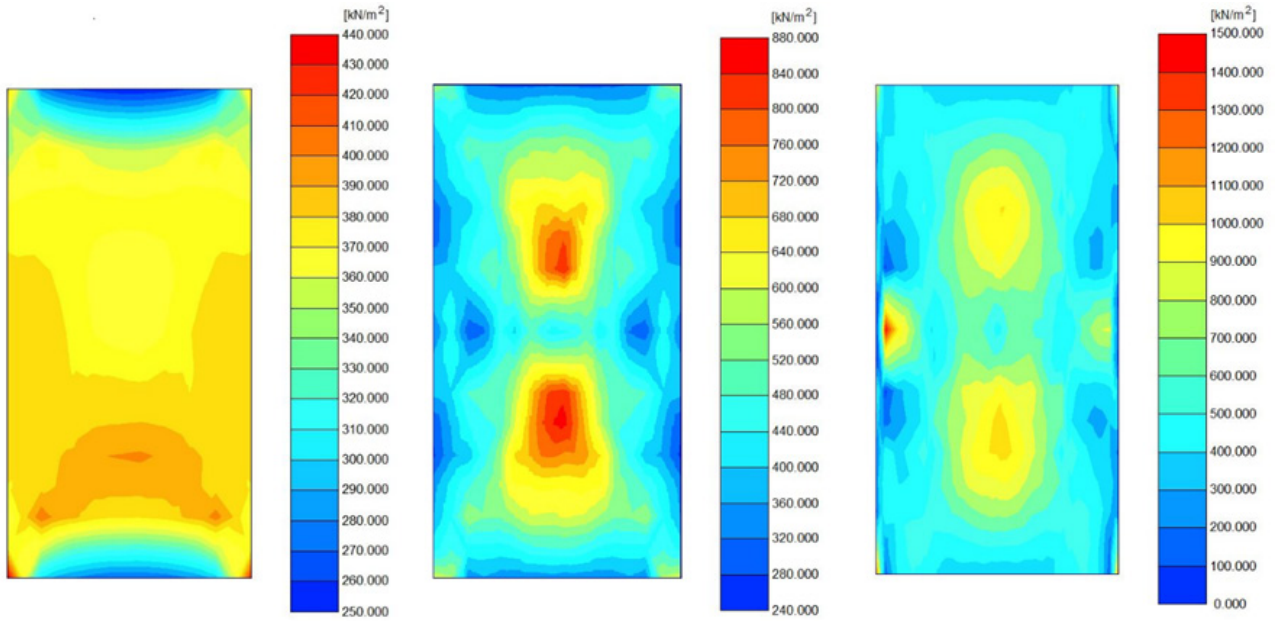

Figure 8: Distribution of stress deviator in vertical cross section when the cell pressure σ_3 = 100 kPa: left – unreinforced sample; middle – sample reinforced with Basetrac® Grid PP 40 geogrid; right – sample reinforced with Basetrac® Grid PET 40 geogrid.

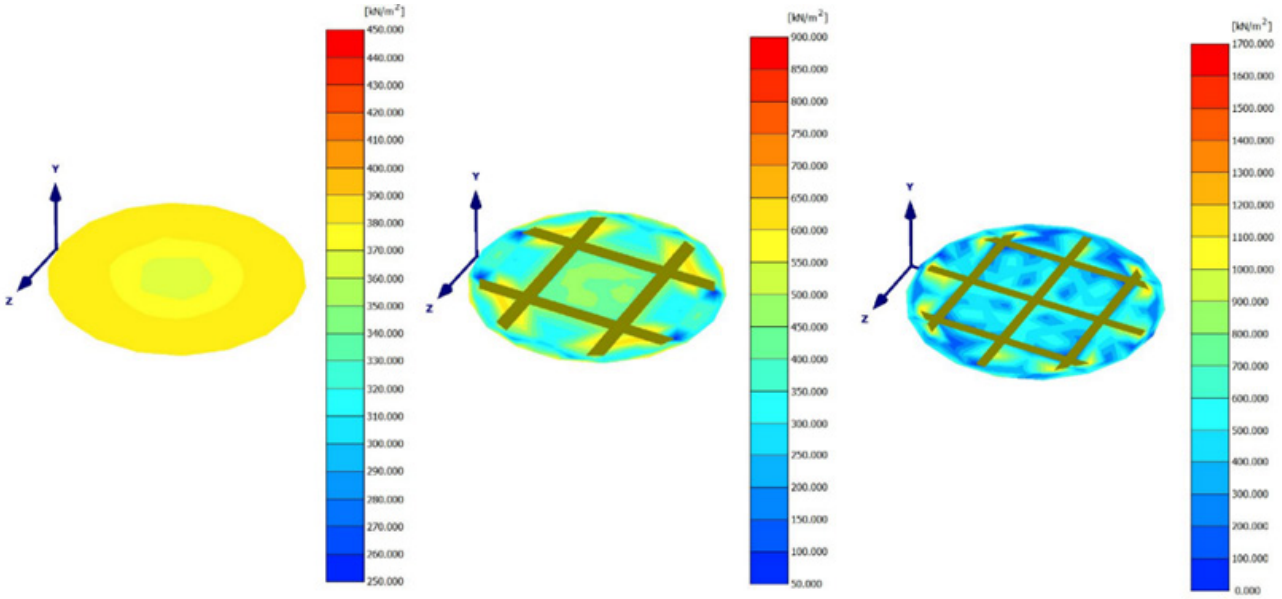

Figure 9: Distribution of stress deviator in the horizontal plane at the geogrid position when the cell pressure σ_3 =100 kPa: left – unreinforced sample; middle – sample reinforced with Basetrac® Grid PP 40 geogrid; right – sample reinforced with Basetrac® Grid PET 40 geogrid.

For both simulated geogrids, bending moments are less than 0.2 kN m and are not actual when compared with tension (Fig. 10) and shear (Fig. 11) forces. Differences in the distribution of shear forces in the geogrids are minimal when the cell pressure is σ_3 = 300 kPa. The maximum concentration of shear forces is at the geogrids' connections and at the ends of geogrids. Concentrations of shear forces for Basetrac Grid PET 40 geogrid explain the damages that occurred during experimental testing (Fig. 7). See Fig. 12 for distribution of volumetric strains in the horizontal plane at the failure stage.

In the evaluation of volumetric strains and when the cell pressure is σ_3 = 300 kPa, the difference between unreinforced samples and samples reinforced with

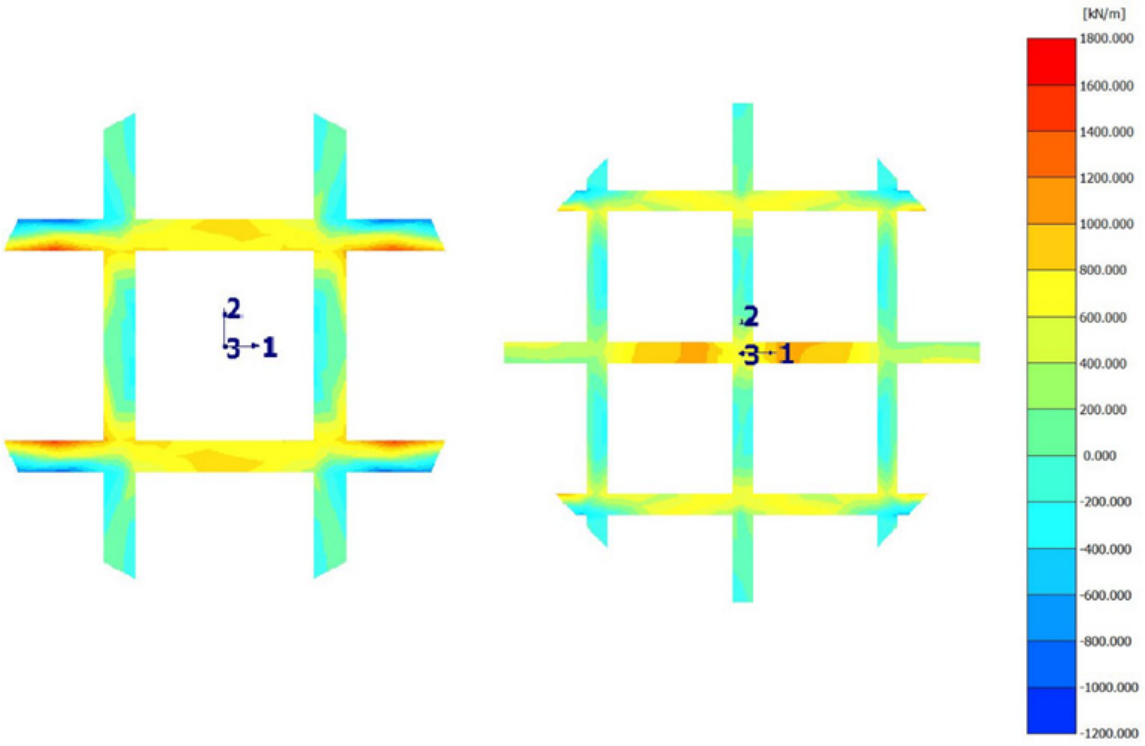

Figure 10: Distribution of tension forces along axis 1 in the geogrids when the cell pressure σ_3 = 300 kPa: left – sample reinforced with Basetrac® Grid PP 40 geogrid; right – sample reinforced with Basetrac® Grid PET 40 geogrid.

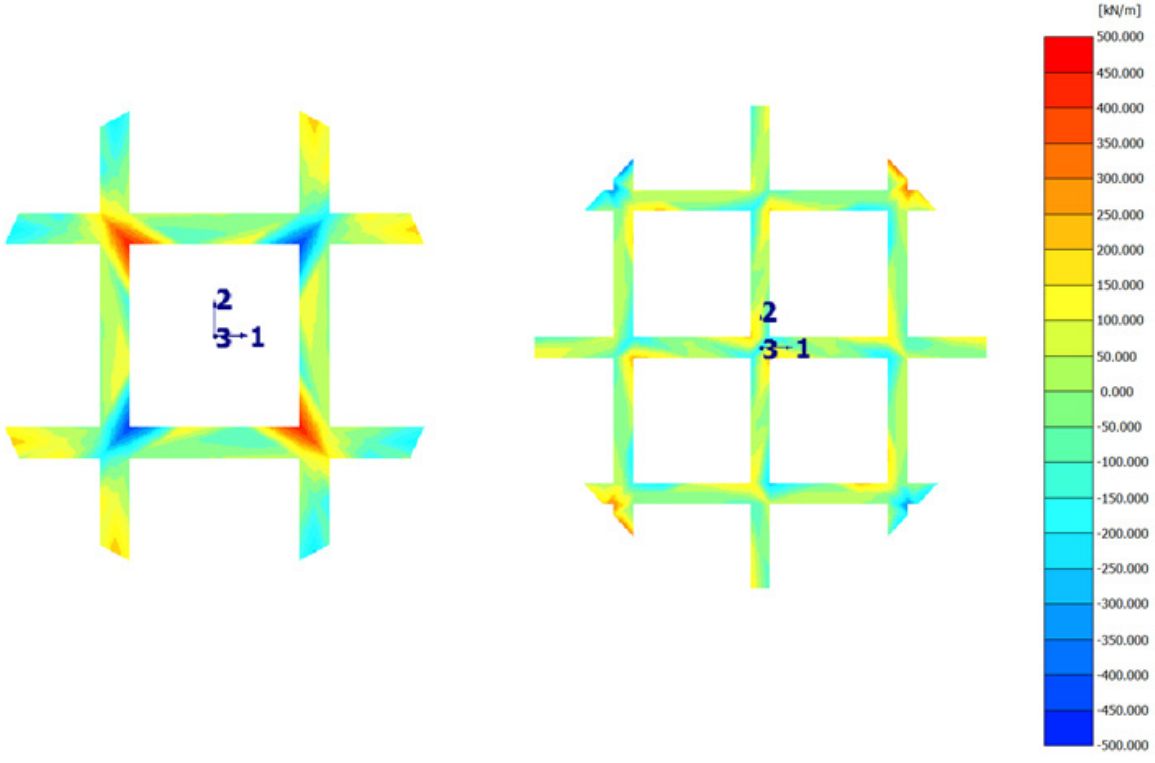

Figure 11: Distribution of shear forces in the geogrids when the cell pressure σ_3 = 300 kPa: left – sample reinforced with Basetrac® Grid PP 40 geogrid; right – sample reinforced with Basetrac® Grid PET 40 geogrid.

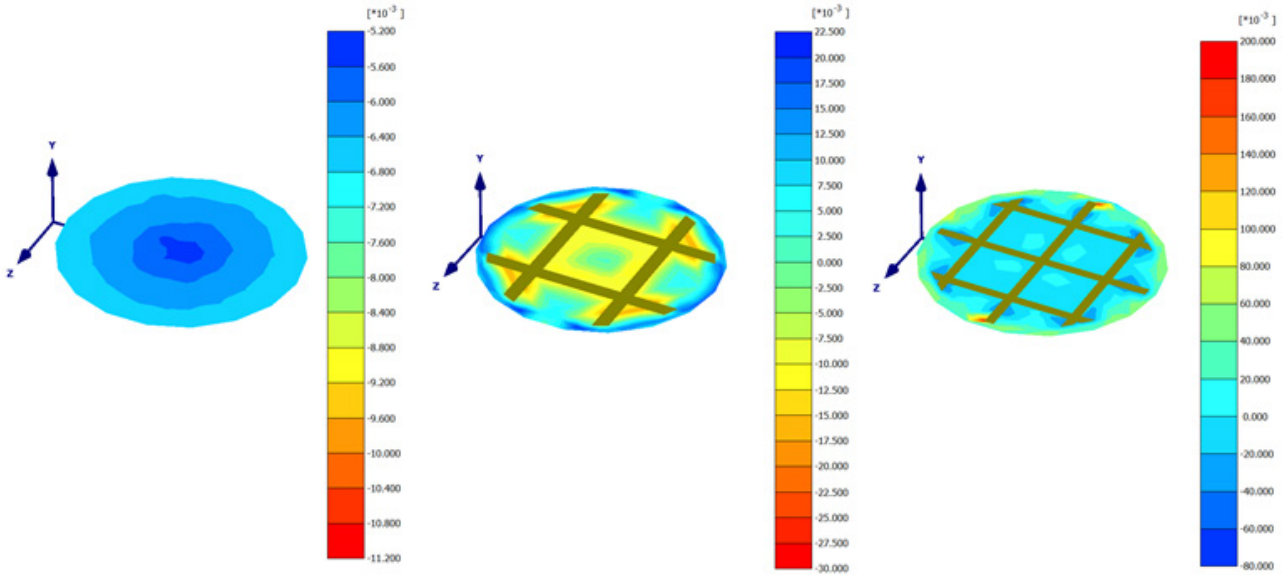

Figure 12: Distribution of total volumetric strains ε_v when the cell pressure σ_3 = 100 kPa: left – unreinforced sample; middle – sample reinforced with Basetrac® Grid PP 40 geogrid; right – sample reinforced with Basetrac® Grid PET 40 geogrid.

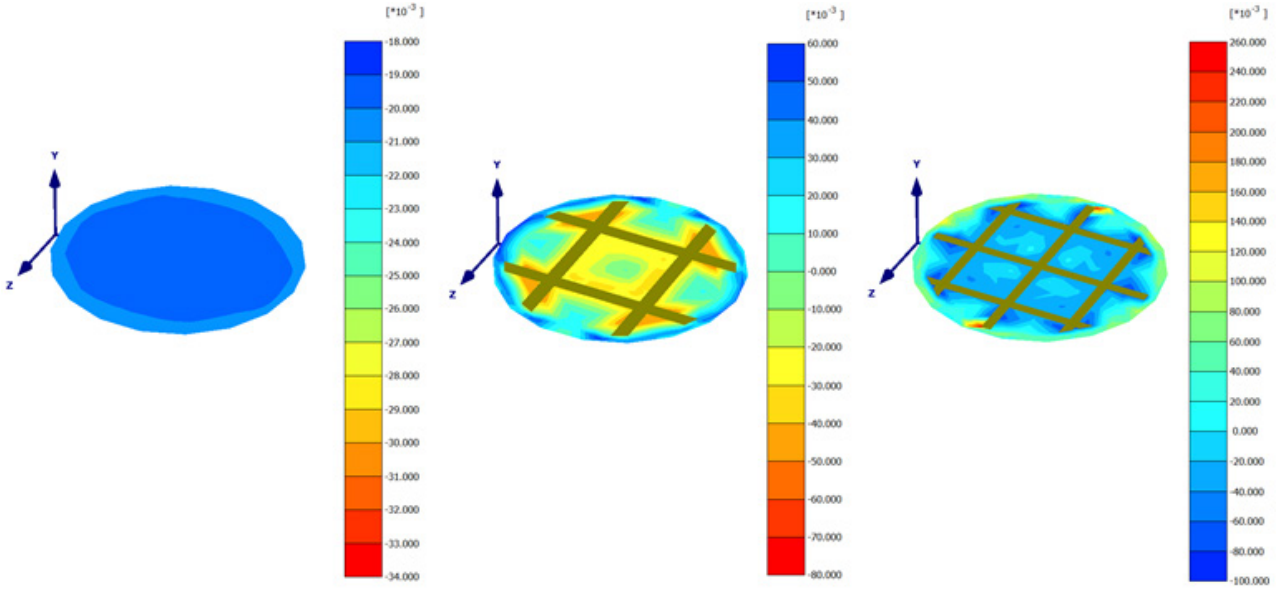

Figure 13: Distribution of total volumetric strains ε_v when the cell pressure σ_3 = 300 kPa: left – unreinforced sample; middle – sample reinforced with Basetrac® Grid PP 40 geogrid; right – sample reinforced with Basetrac® Grid PET 40 geogrid.

geogrids is minimal (see Fig. 13). Volumetric strains vary between 18 × 10^{-3} and 30 × 10^{-3}. Differences in strains between unreinforced samples and samples reinforced with geogrids increase when comparison is made with the cell pressure at σ_3 = 100 kPa. Volumetric strains vary between 5.2×10^{-3} and 40×10^{-3} (see Fig. 12). The distribution of changes in strains can explain experimentally obtained minimal differences in stress deviators (when the cell pressure σ_3 = 300 kPa) between unreinforced samples and samples reinforced with geogrids (see Fig. 6).

Stresses and strains (Figs 8–13) explain the behavior of soil and soil reinforced with geogrids, whereas numerical simulations reveal failure character, which was obtained during experimental testing. Numerical simulations also prove that the quantity of geometry and openings of geogrids are very important for the distribution of stresses and strains in the sample.

5 Conclusions

The following conclusions can be drawn about the reinforcement of samples with geogrids and their influence on triaxial tests results:

(1) Geogrids have a positive influence on the reinforcement of geotechnical constructions. On comparing the shearing strength ratio for reinforced/unreinforced samples, shearing strength increment from 1.09 to 1.43 was obtained for reinforced soil samples.
(2) The angle of internal friction varies from 39.78° to 42.28° for reinforced samples with flexible and rigid geogrids, and it is equal to 40.77° for unreinforced samples. The apparent cohesion in the evaluation of reinforced samples with geogrids has increased up to 43.47 kPa.
(3) Unreinforced soil samples reach peak shearing strength at less than twice the vertical strain compared to reinforced soil samples with geogrids. The fact that the peak shearing strength will be reached at higher strains promotes better design in geotechnical constructions.
(4) In the connections of geogrids, the shearing forces appear. According to the values of shearing forces and the shape of geogrids during experimental testing, some damages appeared only for Basetrac Grid PET 40 geogrid.
(5) When the samples are tested with a high cell pressure (σ_3 = 300 kPa), low efficiency of geogrid reinforcement is obtained in the sample. The difference in the stress deviator at the point of failure is very small in comparison with unreinforced soil sample.

Notwithstanding, it may not be possible to directly apply the results of this research to geotechnical construction design because the research analyzed only the behavior of the soil samples tested with a triaxial test device and this does not validate the scale factor with the polygon testing results. Despite these differences, the test data provide useful and insightful information to gain a better understanding of the behavior and failure mechanism of reinforced soil. The results and discussion in this paper are useful to more clearly understand the shear behavior and stress distribution in soil samples reinforced with geogrids.

Disclosure statement: No potential conflict of interest was reported by the authors.

Funding: This study has been supported by the Lithuanian Agency for Science, Innovation and Technology (MITA), research project number 01.2.1-MITA-K-824.

References

[1] Abdi A., Abbeche K., Athmania D., Bouassida M. (2019) Effective Width Rule in the Analysis of Footing on Reinforced Sand Slope. Studia Geotechnica et Mechanica. Vol. 41, No. 1, 42–55.
[2] Nagy A.C., Moldovan D.-V., Ciotlaus M., Muntean L.E. (2017) Evaluation of Experimental and Numerical Simulation of Triaxial Geogrid Reinforcement on the Strength of Road Structures. Procedia Engineering. 181, 472–479.
[3] Li C., Ashlok J.C., White D.J, Vennapusa P.K.R. (2017) Mechanistic-based comparisons of stabilised base and granular surface layers of low-volume roads. International Journal of Pavement Engineering. Vol. 20, No. 1, 112-124.
[4] Denine S., Della N., Dlawar M. R., Sadok F., Canou J., Dupla J.-C. (2016) Effect of geotextile reinforcement on shear strength of sandy soil. Laboratory study. Studia Geotechnica et Mechanica. Vol. 38, No. 4, 3–13.
[5] Guidelines to use geosynthetics for the roads ground works MN GEOSINT ŽD 13, 2013 [in Lithuanian].
[6] Vaitkus A., Šiukščius A., Ramunas V. (2014) Regulations for use of geosynthetics for road embankments and subgrades. The Baltic journal of road and bridge engineering. Vol. 9, No. 2, 88–93.
[7] Recommendations for design and analysis of earth structures using geosynthetic reinforcements – EBGEO, Translation of the 2nd German Edition, Published by the German Geotechnical Society (Deutsche Gesellschaft Für Geotechnik e.V., DGGT), 2011.
[8] Šiukščius A., Vorobjovas V., Vaitkus, A. (2017) Geogrid reinforced subgrade influence to ensure paved road durability. 10th International conference, "Environmental Engineering", Vilnius Gediminas Technical University, Lithuania. Vilnius: VGTU Press 2017, 1–7.
[9] Nair A. M., Latha G. M. (2014) Large Diameter Triaxial Tests on Geosynthetic-Reinforced Granular Subbases. Journal of Materials in Civil Engineering. Vol. 27, No. 4.
[10] Sakleshpur V.A., Prezzi M., Salgado R., Siddiki N., Choi Y. S. (2019) Large-Scale Direct Shear Testing of Geogrid-Reinforced Aggregate Base over Weak Subgrade. International Journal of Pavement Engineering. Vol. 20, No. 6, 649–658.
[11] Makkar F.M., Chandrakaran S., Sankar N. (2019) Performance of 3-D geogrid-reinforced sand under direct shear mode. International Journal of Geotechnical Engineering. Vol. 13, No. 3.
[12] Yang K.-H., Nguyen M.D., Yalew W.M., Liu C.-N., and Gupta R. (2016) Behavior of Geotextile-Reinforced Clay in Consolidated-Undrained Tests: Reinterpretation of Porewater Pressure Parameters. Journal of GeoEngineering. Vol. 11, No. 2, 45–57.
[13] Da Costa A., Castro J., Sagaseta C., Cañizal J. (2017) Influence of geotextile encasement in triaxial tests on gravel. Proceedings of the 19th International Conference on Soil Mechanics and Geotechnical Engineering, Seoul 2017.

[14] Rezvani R. (2019) Shearing response of geotextile-reinforced calcareous soils using monotonic triaxial tests. Marine Georesources&Geotechnology.
[15] Goodarzi S., Shahnazari H. 2019. Strength enhancement of geotextile-reinforced carbonate sand. Geotextiles and Geomembranes. Vol. 47, No. 2, 128–139.
[16] Amšiejus J., Kačianauskas R., Norkus A., Tumonis L. (2010) Investigation of the sand porosity via oedometer testing. The Baltic Journal of Road and Bridge Engineering. Vol. 5, No 3, 139–147.
[17] Skuodis,Š., Markauskas D., Norkus A., Žaržojus G., Dirgėliene N. (2014) Testing and numerical simulation of Holocene marine sand uniaxial compression at Lithuanian coast. Baltica. Vol. 27, No. 1, 33–44.
[18] ISO 14688-1:2017. Geotechnical Investigation and Testing – Identification and Classification of Soil – part 1: Identification and Description. International Organization for Standardization.
[19] Ojuri O.O., Agbolade O.C. (2015) Improvement of engineering properties of Igbokoda standard sand with shredded polyethylene wastes. Nigeria Journal of Technology. Vol. 34, No. 3, 443–451.
[20] Danesh A., Palassi M., Mirhasemi A.A. (2017) Evaluating the influence of ballast degradation on its shear behaviour. International Journal of Rail Transportation. Vol. 6, No. 3, 145–162.
[21] Sweta K., Hussaini S.K.K. (2018) Effect of shearing rate on the behavior of geogrid-reinforced railroad ballast under direct shear conditions. Geotextiles and Geomembranes. Vol. 46, No 3, 251–256.
[22] Infante D.J.U., Martinez G.M.A., Arrua P.A., Eberhardt M. (2016) Shear strength behaviour of different geosynthetic reinforced soil structure from direct shear test. International Journal of Geosynthetics and Ground Engineering. Vol. 2, No. 17, 1–17.
[23] Han B., Ling J., Shu X., Gong H., Huang B. (2018) Laboratory investigation of particle size effects on the shear behaviour of aggregate-geogrid interface. Construction and Building Materials. 158, 1015–1025.
[24] Gao G., Meguid M.A. (2018) Effect of particle shape on the response of geogrid-reinforced systems: Insights from 3D discrete element analysis. Geotextiles and Geomembranes. Vol. 43, No. 6, 685–698.
[25] Vaitkus A., Čygas D., Laurinavičius A. (2010) Use of geosynthetics for the strengthening of road pavement structure in Lithuania. Geosynthetics for a challenging world: 9th International Conference on Geosynthetics, Guaruja, Brazil, 2010, Vol. 3. San Paulo: Brazilian Chapter of the International Geosynthetics Society (IGS-Brazil), 1575–1580.
[26] Peric D., Su S. (2005) Influence of the end friction on the response of triaxial and plane strain clay samples. Proceedings of the 16th International Conference on Soil Mechanics and Geotechnical Engineering, Osaka, 12–16 September 2005, 571–574.
[27] ISO/TS 17892-9:2004. Geotechnical investigation and testing. Laboratory testing of soil. Part 9: Consolidated triaxial compression tests on water-saturated soils.
[28] Kamel M.A., Chandra S. (2004) Behaviour of subgrade soil reinforced with geogrid. International Journal of Pavement Engineering. Vol. 5, No. 4, 201–209.
[29] Tang H., Zhang X., Ji S. (2017) Discrete element analysis for shear band modes of granular materials in triaxial tests. Particulate Science and Technology. Vol. 35, No. 3, 277–290.
[30] Wang H., Koseki J., Sato T. (2017) p-Constant Condition Applied to Undrained Cyclic Triaxial Test of Unsaturated Soils. Geotechnical Testing Journal. Vol. 40, No. 4, 710–718.
[31] Yang Z.X., Pan K. (2017) Flow deformation and cyclic resistance of saturated loose sand considering initial static shear effect. Soil Dynamics and Earthquake Engineering. 92, 68–78.
[32] Medzvieckas J., Dirgeliene N., Skuodis Š. (2017) Stress-strain states differences in specimens during triaxial compression and direct shear tests. Procedia Engineering. Modern Building Materials, Structures and Techniques, MBMST 2016. Amsterdam: Elsevier Ltd. 172 (2017): 739–745.
[33] Skuodis Š., Dirgėlienė N. (2018) Investigations of soil shear strength reinforced with geogrids, Geologija, Geografija. Vol. 4, No. 2, 59–68 [in Lithuanian].
[34] Strzelecki T., Uciechowska-Grakowicz A., Strzelecki M., Sawicki E., Maniecki Ł. (2018) Numerical 3D simulations of seepage and the seepage stability of the right-bank dam of the Dry Flood Control Reservoir in Racibórz. Studia Geotechnica et Mechanica. Vol. 40, No 1, 11–20.
[35] Brinkgreve R.B.J., AL-Khoury R., Bakker K.J., Bonnier P.G., Brand P.J.W., and Broere W. 2007. PLAXIS 3D Foundation. General Information. Delft University of Technology & PLAXIS bv, The Netherlands.
[36] Bolton M.D. 1986. The Strength and Dilatancy of Sands. Geotechnique. Vol. 36, No. 1, 65–78.
[37] Iwamoto S., Yamamoto S., Lee S-H., Ito H., Endo, T. 2014. Mechanical and Thermal Properties of Polypropylene Composites Reinforced with Lignocellulose Nanofibers Dried in Melted Ethylene-Butene Copolymer. Materials, 7, 6919–6929.
[38] Fu S.-Y., Lauke B., Mai Y.-W. *Science and Engineering of Short Fibre Reinforced Polymer Composites*. 2009. CRC Press Boca Raton USA.